

Vibrationally resolved charge transfer for proton collisions with CO and H collisions with CO⁺

C. Y. Lin* and P. C. Stancil†

Department of Physics and Astronomy and the Center for Simulational Physics, The University of Georgia,
Athens, Georgia 30602-2451, USA

Y. Li, J. P. Gu, H. P. Liebermann, and R. J. Buenker‡

Fachbereich C-Mathematik und Naturwissenschaften, Bergische Universität Wuppertal, D-42097 Wuppertal, Germany

M. Kimura§

Graduate School of Sciences, Kyushu University, Fukuoka 812-8581, Japan

(Received 8 February 2007; published 3 July 2007)

Electron capture by protons following collisions with carbon monoxide, and the reverse process, is studied with a quantal molecular-orbital coupled-channel method utilizing the infinite order sudden approximation for collision energies between 0.5 and 1000 eV/u. The potential surfaces and couplings, computed with the multireference single- and double-excitation method for a range of H⁺-CO orientation angles and C-O separations, are adopted in the scattering calculations. Results including vibrationally resolved and orientation-angle-dependent cross sections are presented for a range of CO and CO⁺ vibrational levels. Comparison with experiment is made where possible and the relevance of the reaction in astrophysics and atmospheric physics is discussed.

DOI: [10.1103/PhysRevA.76.012702](https://doi.org/10.1103/PhysRevA.76.012702)

PACS number(s): 34.10.+x, 34.70.+e, 82.30.Fi

I. INTRODUCTION

Electron capture processes are well-known to be of great interest in many fields of study and are relevant to planetary atmospheres, the interstellar medium, and controlled-thermonuclear fusion. In particular, many investigations are focused on collisions of protons with atoms or molecules, since the major constituent of the solar wind is protons. For example, the interaction of the solar wind with the atmospheres of planets or comets plays a crucial role in understanding x-ray emission from these objects and the interface between the solar wind and their atmospheres. x-ray emission from charge exchange also has the potential to provide information on the composition of the atmospheres and the solar wind.

For the specific case of electron capture by protons in collisions with CO, numerous measurements have been carried out over the past 5 decades [1–6], but the number of theoretical studies [7–9] are sparse. The effect of molecular orientation, the so-called steric effect, for proton-CO collisions was discussed in the theoretical work of Kimura *et al.* [7] and Kumar *et al.* [9]. In Kimura *et al.*, a quantal molecular-orbital coupled-channel (MOCC) calculation was performed which considered three orientation angles ($\Theta = 0^\circ, 90^\circ, \text{ and } 180^\circ$) of the target molecule. However, CO was held fixed at its equilibrium distance $r_e = 2.1a_0$ throughout the collision; the so-called “electronic approximation” (EA). Kumar *et al.* also performed an EA calculation, but with a time-dependent wave-packet propagation (TDWP)

method. In a preliminary investigation [8], we relaxed this restriction and considered vibrational motion of CO. This allows us to compute vibrationally resolved cross sections within the infinite order sudden approximation (IOSA) [10,11] and to demonstrate that an EA calculation is inappropriate for collision energies less than ~ 100 eV/u.

Extending our earlier investigation [8], the present work includes a significant enhancement in the CO and CO⁺ vibrational bases in order to provide more accurate and more extensive information on vibrationally resolved electron capture. The collision process considered in this work is



which is endoergic by 0.416 eV for $\nu = \nu' = 0$ for the forward direction. The potentials and couplings in the adiabatic and diabatic representation for three collision configurations are discussed in Sec. II. We briefly describe the theoretical approach for the scattering calculations in Sec. III. The results of state-to-state, state-selective, and angle-averaged total cross sections are illustrated in Sec. IV including the discussion and comparison with the existing experimental data and previous calculations. Section V addresses the implications

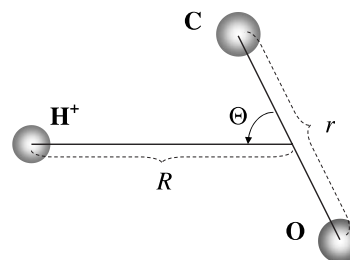


FIG. 1. The collisions of H⁺ with CO defined in the Jacobi coordinate system.

*Electronic address: cylin@hal.physast.uga.edu†Electronic address: stancil@physast.uga.edu‡Electronic address: buenker@uni-wuppertal.de§Electronic address: mineoscc@mbox.nc.kyushu-u.ac.jp

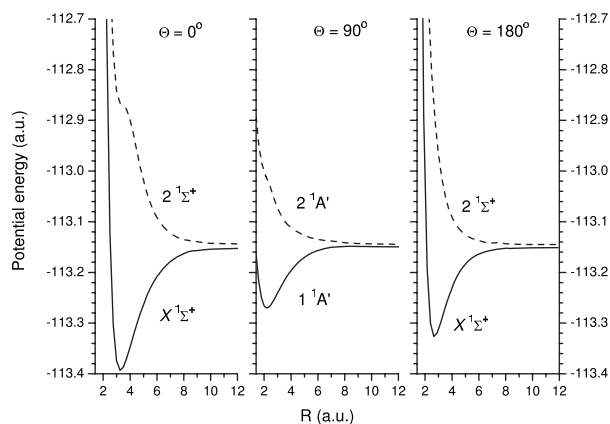


FIG. 2. Adiabatic potential curves as functions of R with $r=r_e$.

to astrophysics and atmospheric physics from the current results, while Sec. VI briefly gives the summary of the present investigations. Atomic units are used throughout unless otherwise noted.

II. ELECTRONIC STRUCTURE CALCULATIONS

Ab initio calculations were performed for the potential surfaces and coupling matrix elements of the HCO^+ molecular ion. The calculations were carried out using the multireference single- and double-excitation (MRD-CI) method [12–17] with the cc-pVTZ basis for H, C, and O atoms of Dunning [18]. In this work we consider three collision configurations defined in Fig. 1 with $\Theta=0^\circ, 90^\circ$, and 180° . For each Θ , the adiabatic potentials and couplings as functions of the H-CO internuclear distance R are computed with five different fixed C-O internuclear separations of $r=1.7, 1.9, 2.1, 2.3$, and $2.5a_0$, where $2.1a_0$ is the equilibrium distance of the CO molecule. For the collision energy computed in this work, we consider the two lowest electronic states only as the remaining excited states are more than 2.5 eV higher in energy and therefore of secondary importance in the collision dynamics. The two lowest potentials, with CO at its equilibrium geometry $r=r_e$, are shown in Fig. 2 and correspond to the asymptotes $\text{H}^+ + \text{CO}(X^1\Sigma^+)$ and $\text{H} + \text{CO}^+(X^2\Sigma^+)$. For $\Theta=0^\circ$ and 180° , the $X^1\Sigma^+$ and $2^1\Sigma^+$ states were computed in the C_{2v} subgroup of the $C_{\infty v}$ point group, while for $\Theta=90^\circ$, the $1^1A'$ and $2^1A'$ were calculated in the C_s point group [7]. The nuclear radial coupling matrix elements, which connect these two states, are displayed as functions of R and various r in Fig. 3 for three different collision geometries.

For convenience in the scattering calculations, we make a unitary transformation from the adiabatic picture to a diabatic representation for the electronic potentials and couplings. The resulting diagonal terms of the electronic diabatic potentials are adjusted to match the experimental asymptotic energies for $\nu=\nu'=0$. The vibronic diabatic potential energies are then obtained by shifting the appropriate electronic energy by the vibrational excitation energies as shown in Fig. 4. The vibronic diabatic couplings are obtained by averaging the electronic diabatic couplings over the vibrational wave

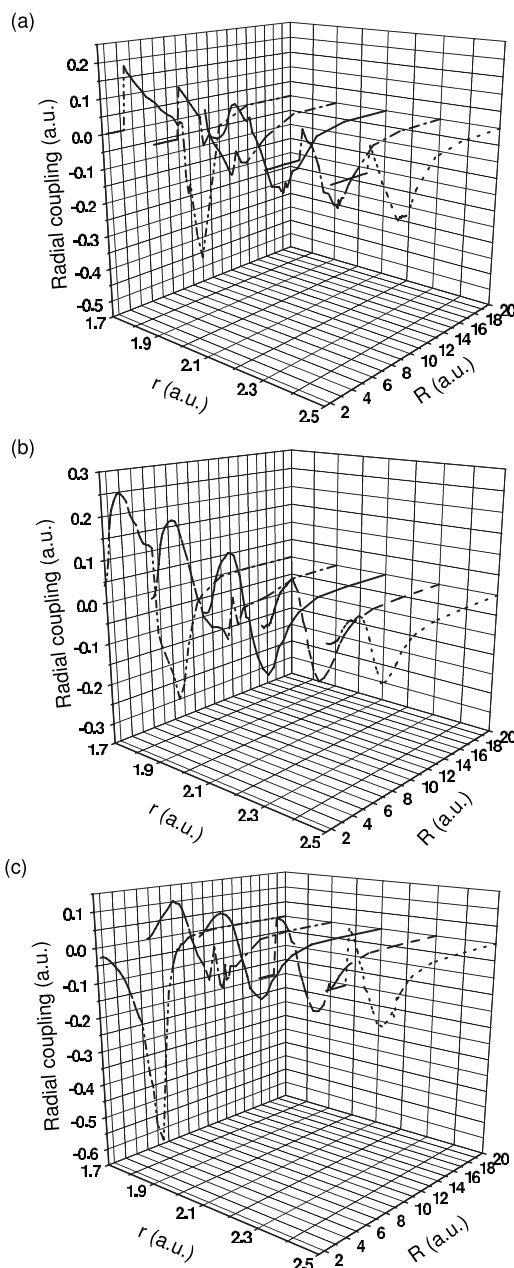


FIG. 3. Adiabatic radial couplings as functions of R with $r=1.7, 1.9, 2.1, 2.3$, and $2.5a_0$ for $\Theta=(a) 0^\circ, (b) 90^\circ$, and $(c) 180^\circ$.

functions as in Eq. (4). The dominant vibronic couplings are shown in Fig. 5 for transitions connecting the states ν with $\nu'=\nu$ and $\nu\pm 1$. The vibronic couplings for larger $|\Delta\nu|$ are significantly smaller. The CO^+ and CO ground state potentials, used to generate the vibrational wave functions, were taken from Krupenie and Weissman [19] and Borges *et al.* [20], respectively.

III. SCATTERING THEORY

The MOCC approach has been applied to several cases of electron capture in proton collisions with atoms, including, for example, N [21], S [22], O [23], and C [24]. Here, we extend it to the more complicated case of a molecular target.

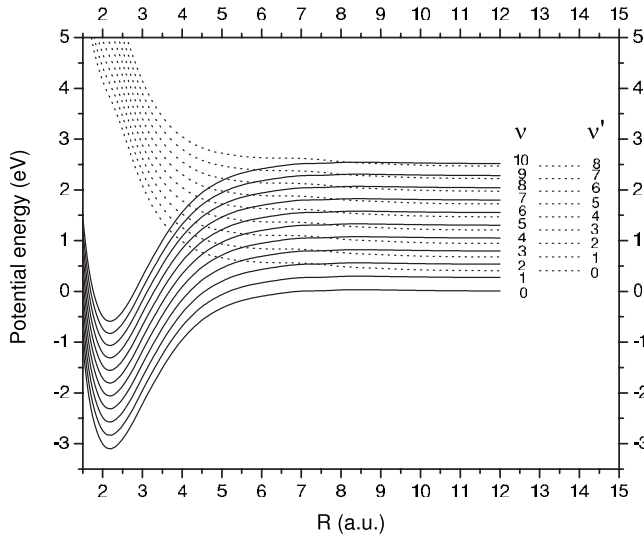


FIG. 4. Diabatic potentials as functions of R for the vibronic states of $\nu=0-10$ shifted from $1^1A'$ and $\nu'=0-8$ from $2^1A'$ at $\Theta=90^\circ$ with $r=r_c$.

The method generally follows the formalism of Zygelman *et al.* [25,26], but is expanded to treat molecular targets as outlined by Sidis [10,27] adopting the IOSA. Since the details have been described previously [8,28], only a brief outline is given here.

For an ion-molecule collision system, it is conventional to adopt body-fixed Jacobi coordinates (R, r, Θ) as in Fig. 1, where R is the internuclear distance from the center of mass of the target molecule to the projectile ion, r the stretching distance of the diatom, and $\hat{R} \times \hat{r} = \cos \Theta$. The total wave function for the Schrödinger equation for this collision sys-

tem in the perturbed stationary state expansion is expressed as

$$\Psi(\mathbf{R}, \mathbf{r}, \{\rho_i\}) = \sum_{\gamma} N_{\gamma}(\mathbf{R}, \mathbf{r}) \Phi_{\gamma}(\{\rho_i\}; \mathbf{R}, \mathbf{r}), \quad (2)$$

where ρ_i is the position vector of the electron in the body-fixed frame, N_{γ} is the nuclear wave function, and Φ_{γ} is the electronic wave function for electronic state γ . In the EA, which only considers the transitions between electronic states, the nuclear wave function N_{γ} is a function of R and Θ , while the diabatic couplings $V_{\gamma, \gamma'}^d$ are independent of r . For the present work within IOSA, the nuclear wave functions are expanded over a basis of vibrational states ν , i.e.,

$$N_{\gamma}(\mathbf{R}, \mathbf{r}) = \sum_{\nu} F_{\gamma\nu}(\mathbf{R}) \frac{\chi_{\gamma\nu}(r)}{r} |j_{\gamma}, m_{j_{\gamma}}\rangle, \quad (3)$$

where $\chi_{\gamma\nu}(r)$ are the vibrational wave functions of the diatom, either CO or CO⁺, and the rotational quantum number j_{γ} for the rotational wave function $|j_{\gamma}, m_{j_{\gamma}}\rangle$ of the diatom is taken to be zero. Here, the energy sudden approximation is adopted which assumes that the diatom does not rotate during the collision. The corresponding electronic couplings are therefore r -dependent. The dependence on the vibrational coordinate is removed by averaging over r with the vibrational wave functions of the diatoms to obtain the vibronic couplings (in the diabatic representation)

$$V_{\gamma\nu, \gamma'\nu'}^d(R, \Theta) = \langle \chi_{\gamma\nu}(r) | V_{\gamma, \gamma'}^d(R, r, \Theta) | \chi_{\gamma'\nu'}(r) \rangle, \quad (4)$$

with dominant vibronic couplings shown in Fig. 5.

With the vibronic couplings driving transitions between vibronic states, vibrationally resolved state-to-state cross sections $\sigma_{\gamma\nu, \gamma'\nu'}(\Theta)$ are expressed in terms of S -matrix elements

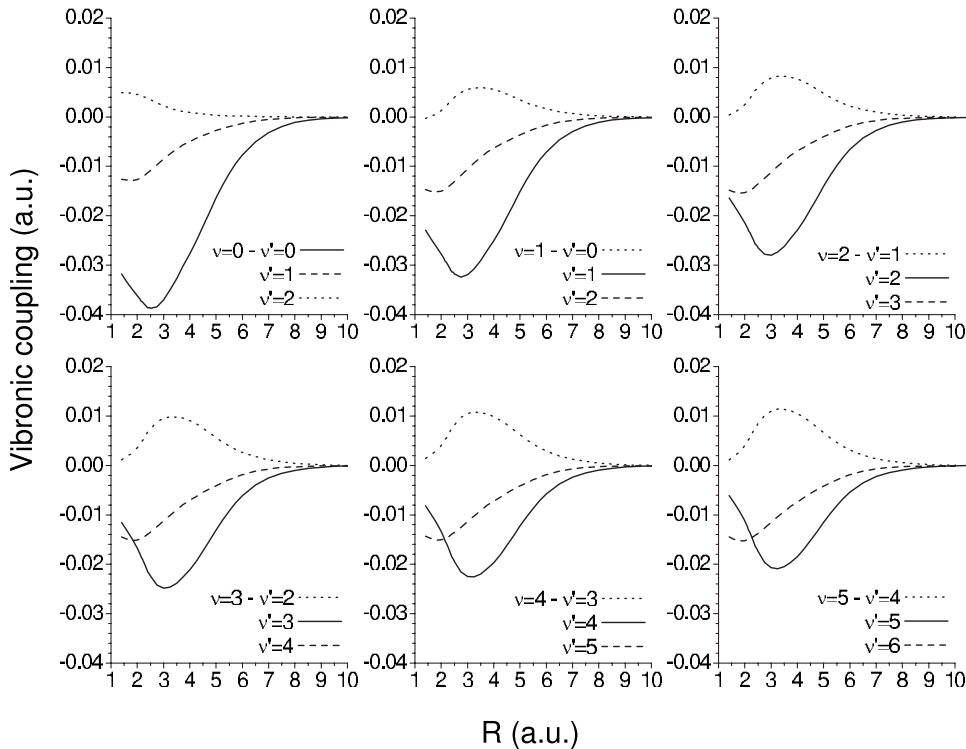


FIG. 5. Vibronic couplings for $\Theta=90^\circ$ as functions of R connecting states $\nu=0-5$ with states $\nu' = \nu$ and $\nu \pm 1$.

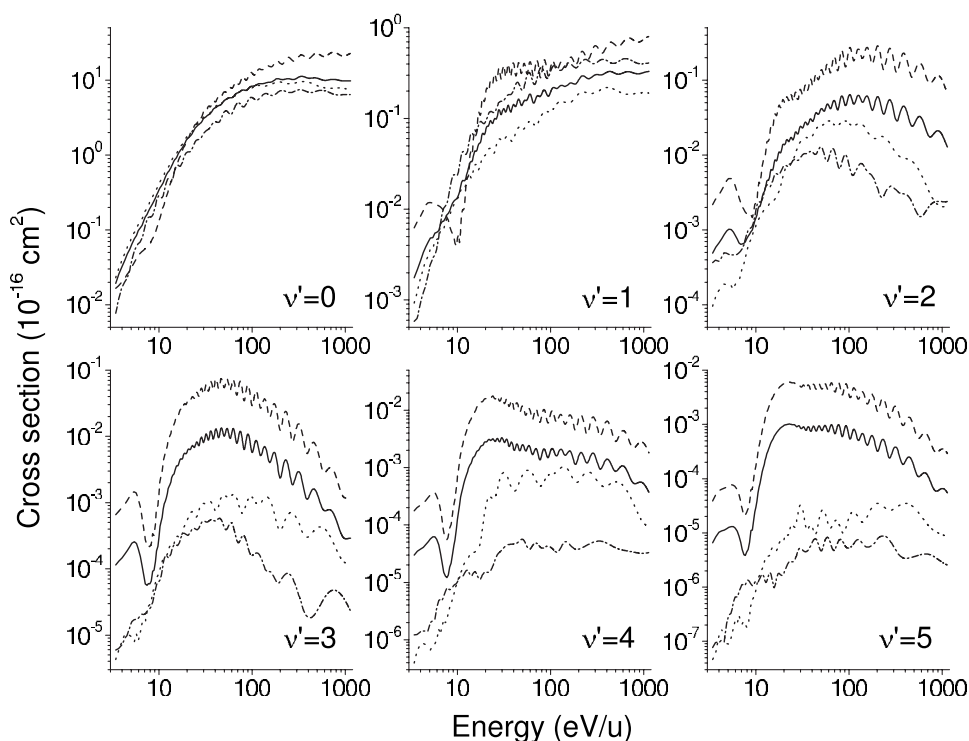


FIG. 6. State-to-state cross sections for $\text{H}^+ + \text{CO}(\nu=0) \rightarrow \text{H} + \text{CO}^+(\nu'=0-5)$ with dashed lines for $\Theta=0^\circ$, dotted lines for $\Theta=90^\circ$, dash-dotted lines for $\Theta=180^\circ$, and solid lines for angle-averaged.

$$\sigma_{\gamma\nu, \gamma' \nu'}(\Theta) = \frac{\pi g_{\gamma\nu}}{k_{\gamma\nu}^2} \sum_J (2J+1) |S_{\gamma\nu, \gamma' \nu'}^J(\Theta)|^2, \quad (5)$$

where $k_{\gamma\nu}$ denotes the wave number for the center-of-mass motion of the initial incoming channel and $g_{\gamma\nu}$ is the initial approach probability factor for the electronic state. To obtain the S -matrix elements, the centrifugal sudden approximation, which neglects the rotation in space of the body-fixed coordinates, has been adopted. The angle Θ is therefore assumed to remain constant throughout the collision. The combination of the centrifugal and energy sudden approximations is IOSA, which has been extensively used in studies of rovi-

brational excitation. Initial state-selective cross sections are given by

$$\sigma_{\gamma\nu}(\Theta) = \sum_{\gamma' \nu'} \sigma_{\gamma\nu, \gamma' \nu'}(\Theta). \quad (6)$$

For comparison with experimental data, the population of the initial vibrational states is determined with a Boltzmann distribution for a given molecular gas temperature T . The total cross section as a function of orientation angle Θ and T are given by

$$\sigma(\Theta, T) = \frac{\sum_{\gamma\nu} \exp(-E_{\gamma\nu}/k_b T) \sigma_{\gamma\nu}(\Theta)}{\sum_{\gamma\nu} \exp(-E_{\gamma\nu}/k_b T)}, \quad (7)$$

where $E_{\gamma\nu}$ are the excitation energies of CO or CO^+ and k_b the Boltzmann constant. In the present calculations, we adopt $T=300$ K. As the scattering calculations are performed for a fixed orientation angle, the angle-averaged cross sections are obtained by [11]

$$\sigma = \frac{1}{2} \int_0^\pi \sigma(\Theta) \sin \Theta d\Theta. \quad (8)$$

IV. RESULTS AND DISCUSSION

The charge exchange cross sections for collisions of H^+ with CO and H with CO^+ were calculated for three orientations, i.e., $\Theta=0^\circ$, 90° , and 180° , of the molecular target and included 11 and 9 vibrational channels for CO and CO^+ , respectively. Examples of vibrationally resolved state-to-state cross sections for H^+ -CO collisions for $\nu=0 \rightarrow \nu'$

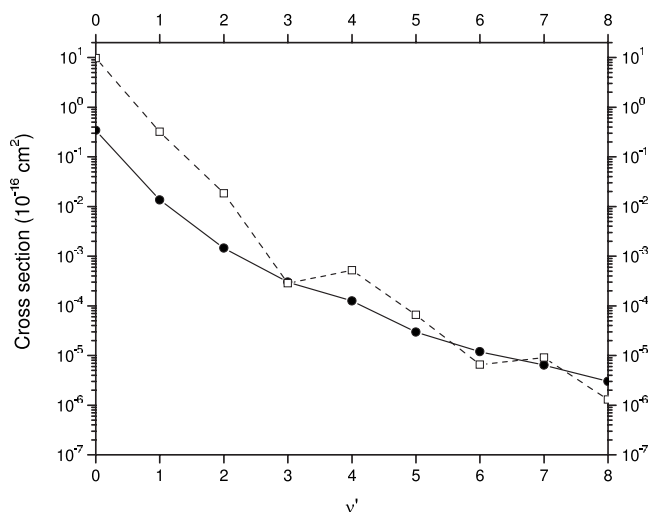


FIG. 7. Angle-averaged state-to-state cross sections of $\text{H}^+ + \text{CO}(\nu=0) \rightarrow \text{H} + \text{CO}^+(\nu'=0-8)$ for 9.96 eV/u (circle-solid line) and 1001.50 eV/u (square-dashed line).

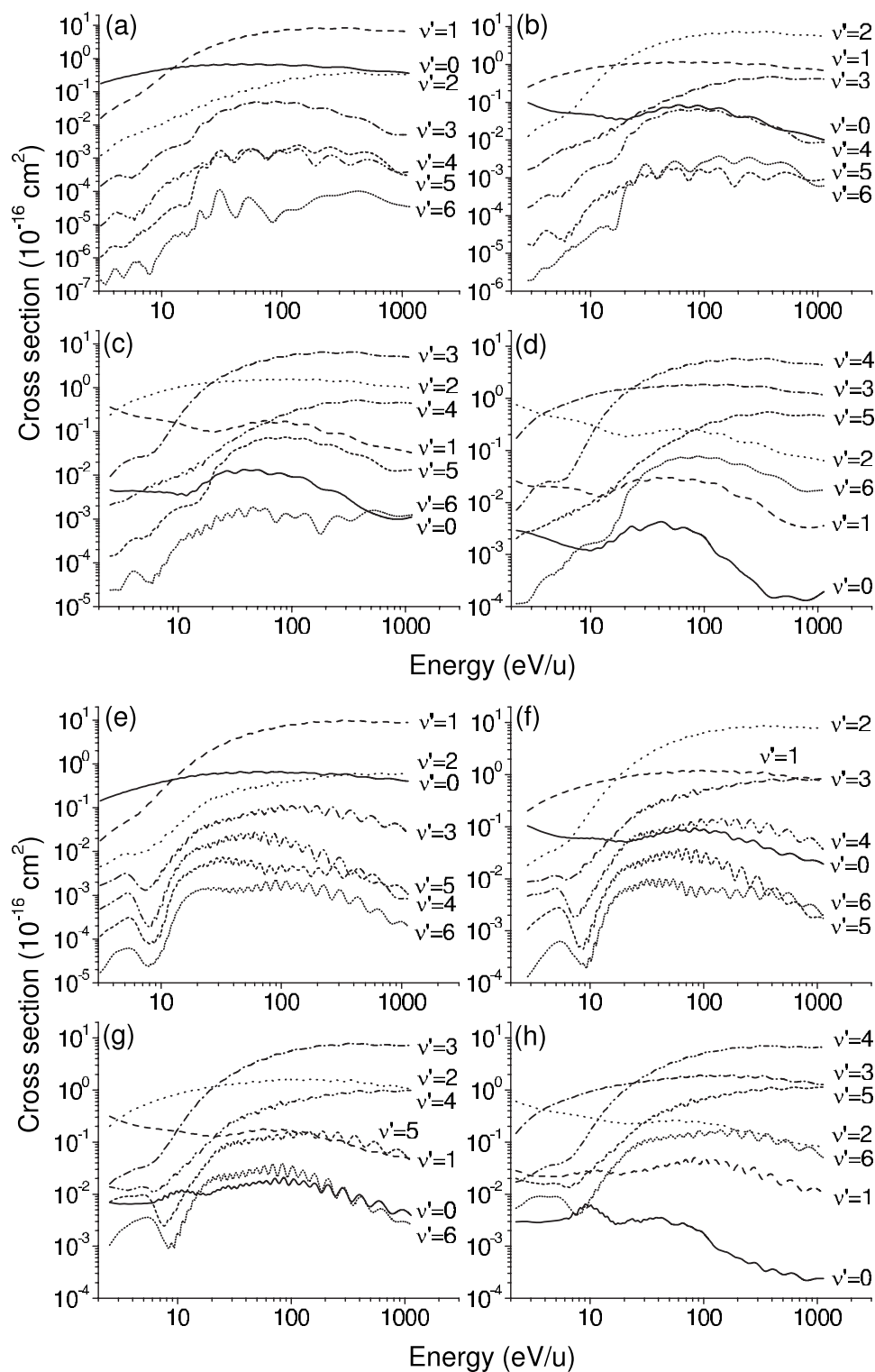


FIG. 8. State-to-state cross sections of $\text{H}^+ + \text{CO}(\nu) \rightarrow \text{H} + \text{CO}^+(\nu'=0-6)$ for $\Theta=90^\circ$: (a) $\nu=1$, (b) $\nu=2$, (c) $\nu=3$, and (d) $\nu=4$, and for angle-averaged: (e) $\nu=1$, (f) $\nu=2$, (g) $\nu=3$, and (h) $\nu=4$.

$\nu=0-5$ are illustrated in Fig. 6. The difference in the cross sections among three angles becomes more conspicuous with increasing final vibrational excitation. For $\nu' \geq 2$, the angle-averaged results are primarily determined by the behavior of the $\Theta=0^\circ$ cross sections. In Fig. 7, angle-averaged state-to-state cross sections for $\nu=0$ are given as a function of ν' for two collision energies. The $\Delta\nu=0$ transition is shown to be the dominant process which is a consequence of the

dominance of the corresponding vibronic coupling. Further, since the vibronic couplings diminish with increasing ν' , the cross sections tend to decrease as well. This behavior is directly related to the overlap of the initial CO and final CO^+ vibrational wave functions which is nearly diagonal since the equilibrium separations of the two molecules are very similar. This suggests that to a rough approximation, the so-called centroid approximation (CA), where a purely elec-

tronic cross section is multiplied by Franck-Condon-like ionization factors, is valid for this collision system for collision energies above ~ 100 eV/u.

State-to-state cross sections for H^+ -CO collisions with $\Theta=90^\circ$ and $\nu>0$ are shown in Figs. 8(a)–8(d). In the high energy regime, the transition from the initial vibronic state ν to a final vibronic state $\nu'=\nu$ is the most dominant process, while in the low energy limit, i.e., near the threshold, the most significant process is a transition to a final vibronic state which is the nearest state in the asymptotic limit. Referring to the vibronic couplings in Fig. 5, it is obviously illustrated that the most important coupling connects two vibronic states of $\nu=\nu'$. However, since the couplings are largest at short R and the final vibronic potentials are repulsive (see Fig. 4), the peaks in the couplings are only sampled for relatively large collision energies. For example, in Fig. 8(a) the cross section for $\nu=1 \rightarrow \nu'=1$ increases with collision energy to become the dominant channel above 10 eV/u. For smaller collision energies, capture to $\nu'=0$ is the primary channel due to a smaller energy gap. For $\nu=2$ similar trends are seen in Fig. 8(b) with the largest cross section to $\nu'=2$ for energies larger than ~ 10 eV/u and to $\nu'=1$ for smaller energies. Capture to $\nu'=0$ is also seen to be significant at low energies and will likely become the dominant channel for energies below the $\nu'=1$ threshold since it is the only exoergic channel. Analogous behavior is seen for other initial ν states. Angle-averaged state-to-state cross sections of H^+ -CO collisions are shown in Figs. 8(e)–8(h), which are dominated by collisions at $\Theta=0^\circ$ for the same reasons as discussed in Fig. 6. The behavior of the different ν and ν' channels are the same as presented above.

The initial state-selective cross sections ($\nu=0-10$), given by Eq. (6), for $\Theta=90^\circ$ collisions of H^+ with CO are displayed in Fig. 9(a). According to the state-to-state cross sections, the convergence of initial state-selective cross sections with respect to the present final states included is reliable except for $\nu=8, 9$, and 10, for which more vibronic states are likely needed. For low energies, the initial state-selective cross sections increase with increasing ν . Because all final states are endoergic for $\nu=0$ and 1 (see Fig. 4), the cross sections are expected to drop sharply due to the threshold. For $\nu>1$, exoergic channels become available which result in the rise of the cross sections. This behavior is also equally applicable to the cases of $\Theta=0^\circ$ and 180° . For the higher energy region, i.e., energies larger than ~ 70 eV/u for the case of $\Theta=90^\circ$, the cross sections increase with decreasing ν . For $\Theta=0^\circ$ and 180° and energies larger than ~ 30 eV/u, the initial state-selective cross sections approach values of similar magnitude. The angle-averaged initial state-selective cross sections are shown in Fig. 9(b), which except for $\nu=9$ and 10, are weakly dependent on ν for energies greater than 50 eV/u.

Figures 10–12 are similar to Figs. 7–9, except for the reverse process of H collisions with CO^+ . Figure 10 shows angle-averaged state-to-state cross sections which have behaviors similar to H^+ -CO, except that exoergic channels are available for all initial states. As discussed previously, $\nu'=\nu$ transitions eventually become the most important as long as the collision energy is large enough. A comparison of final CO vibrational cross sections at relatively high

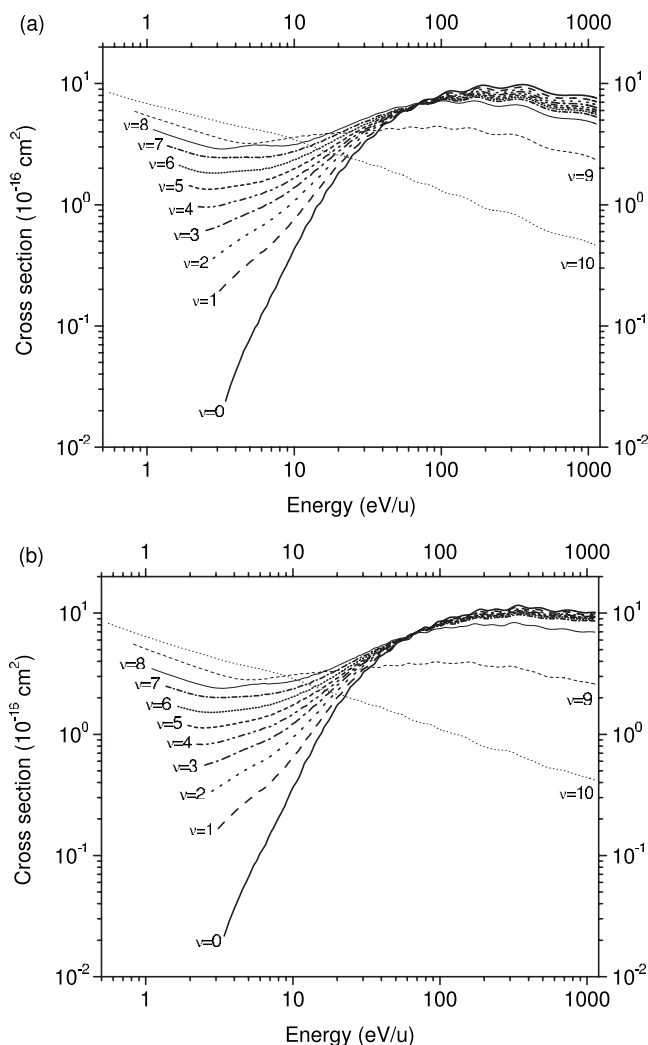


FIG. 9. Initial state-selective cross sections of H^+ collisions with CO [(a) $\Theta=90^\circ$ and (b) angle-averaged] for initial states of $\nu=0-10$.

(~ 1 keV/u) and low (~ 10 eV/u) collision energy is presented in Fig. 11. Generally, a CA-type trend is evident except at low energy where the capture to $\nu=0$ and 1 are nearly equal. The latter is a result of competition between coupling strengths and asymptotic energy gaps. Initial state-selective cross sections for $\Theta=90^\circ$ are shown in Fig. 12(a). The dominant initial state for electron capture is $\nu'=0$ in the high energy regime while the cross section decreases with increasing ν' . For the low energy region, capture from larger ν' becomes more important. In addition, because there are exoergic collision channels involved in the electron capture process for any initial state ν' , all cross sections are expected to rise as the energy approaches zero. In Fig. 12(b), angle-averaged initial state-selective cross sections are presented which demonstrate some dependence of orientation angle by the comparison with Fig. 12(a).

In Fig. 13, orientation-angle-dependent and orientation-angle-averaged total cross sections for single electron capture by protons with CO are displayed and compared with other theoretical and experimental data. The calculations include a Boltzmann average of initial vibrational states at

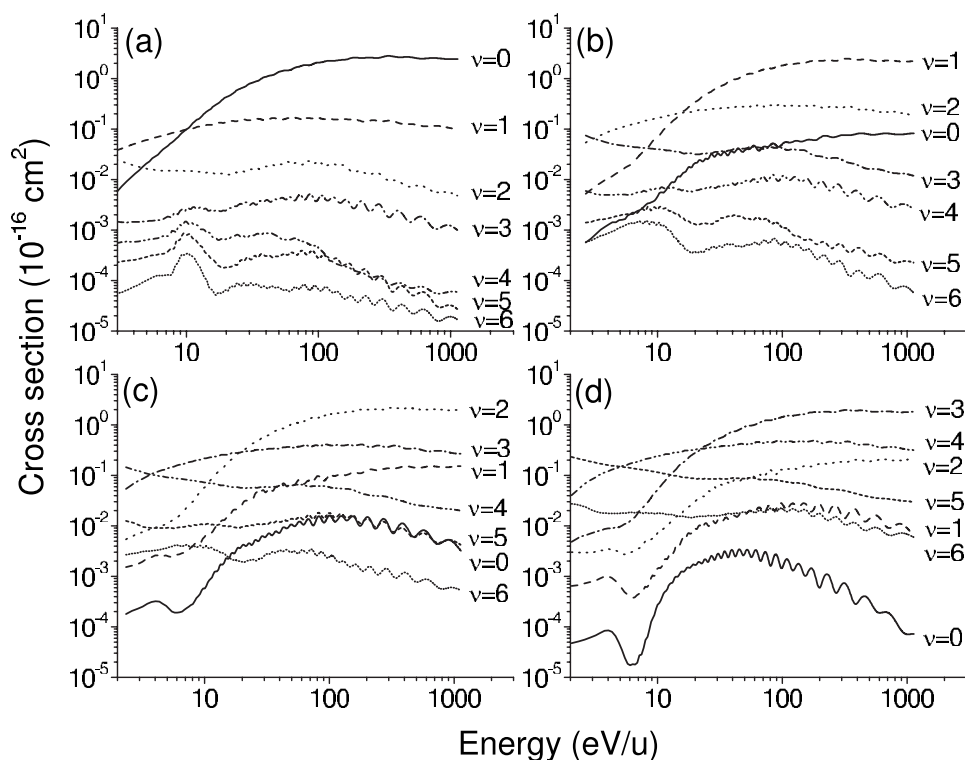


FIG. 10. Angle-averaged state-to-state cross sections of $\text{H} + \text{CO}^+(\nu') \rightarrow \text{H}^+ + \text{CO}(\nu=0-6)$ for (a) $\nu'=0$, (b) $\nu'=1$, (c) $\nu'=2$, and (d) $\nu'=3$.

300 K using Eq. (7). The orientation effect of the target molecule CO is elucidated through cross sections at the three specific angles. It is obvious that $\Theta=0^\circ$ has the largest cross section, compared to the other two angles for energies larger than ~ 20 eV/u. The experimental results of Gao *et al.* [4], Kusakabe *et al.* [5], and Cadez *et al.* [6] were primarily measured for energies near or larger than 1 keV/u. For smaller energies, we are only aware of the measurements of Gilbody *et al.* [1] and Gustafsson *et al.* [2]. The current orientation-angle-averaged total cross sections are in generally good agreement with the other theoretical and experimental data. The discrepancies between the present IOSA

results and the previous EA calculation [8], which neglected vibrational motion, illustrate the significant vibrational effect for the low energy regime. The current IOSA results are generally smaller than the measurements which may be due to the limited number of considered orientation angles or missing contributions from higher excited states. However, we expect the variation in the total cross section with orientation angle to be representative of the uncertainty of our results at a particular collision energy. The orientation-angle-dependent and orientation-angle-averaged total cross sections for H-CO⁺ collisions are displayed in Fig. 14. Comparing to Fig. 13, the results of H-CO⁺ collisions in the high-energy region have a similar trend to H⁺-CO. Electron capture through the collisions with $\Theta=0^\circ$ are most significant, while $\Theta=180^\circ$ has less contribution. We are unaware of other theoretical or experimental results in this collision energy range for this system.

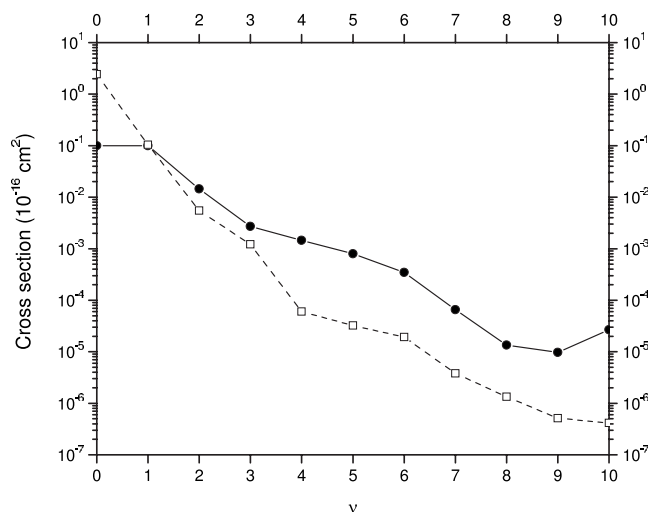


FIG. 11. Angle-averaged state-to-state cross sections of $\text{H} + \text{CO}^+(\nu'=0) \rightarrow \text{H}^+ + \text{CO}(\nu=0-10)$ at 10.06 eV/u (circle-solid line) and at 1001.03 eV/u (square-dashed line).

V. ASTROPHYSICAL AND ATMOSPHERIC APPLICATIONS

CO is typically the second most abundant molecule, after molecular hydrogen, in a variety of astrophysical objects including interstellar clouds. In comets, CO accounts for about 15% of the gaseous material in the coma with the remainder due mostly to water. As a comet travels through the solar system, it encounters the solar wind which is composed primarily of protons with kinetic energies ranging from 0.2 to 3 keV/u. Collisions of CO with solar wind protons are the dominant mechanism for producing CO⁺, which are observed in fluorescence in comet tails [29], since solar photoionization is inefficient. As indicated in Fig. 6, CO⁺ is predominately created in the ground vibrational state. Fur-

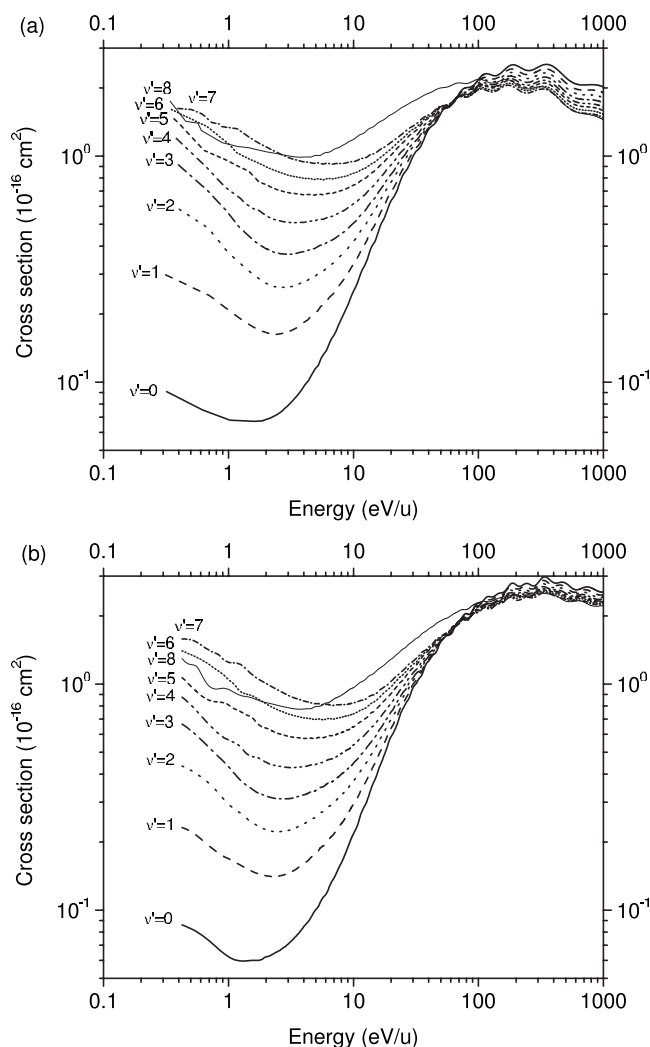


FIG. 12. Initial state-selective cross sections of H collisions with CO^+ [(a) $\Theta=90^\circ$ and (b) angle-averaged] for initial states of $\nu' = 0-8$.

ther, in our previous study, it was found that electron capture to electronically excited CO^+ has a cross section more than two orders of magnitude smaller than the ground state [7]. Therefore while charge transfer creates CO^+ , the observed fluorescence is likely produced following electron-impact or solar photon excitation. Charge exchange also results in a loss of protons, a process observed in the coma of comet Halley, but previous models only considered proton charge exchange with water [30].

The reverse process of H collisions with CO^+ may play a role in the chemistry of diffuse interstellar clouds. Federer *et al.* [3] measured the rate coefficient to be 40% of the Langevin value for a collision energy of 0.06 eV. This energy is too low for the IOSA to be applicable, but if the trend indicated in Fig. 10(a) holds to low energies, the current results suggest that the charge transfer reaction $\text{H}+\text{CO}^+$ would produce CO in $\nu=1$ and 2 even in very cold environments.

VI. SUMMARY

Calculations for electron capture during proton collisions with CO and H collisions with CO^+ have been performed for

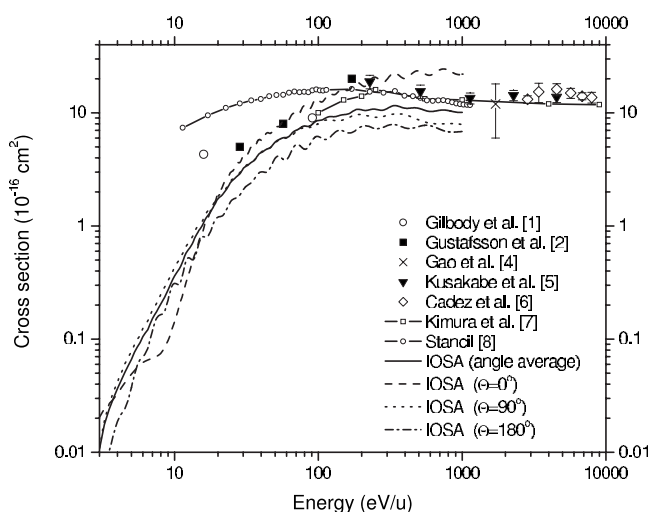


FIG. 13. Orientation-angle-averaged and orientation-angle-dependent total cross sections for the collisions of H^+ with CO compared with previous theoretical and experimental data.

energies between 0.45 eV/u and 1 keV/u using the molecular-orbital coupled-channel approach with the infinite order sudden approximation. The adiabatic potential curves and nonadiabatic radial couplings were obtained with the MRD-CI method. Taking into account the vibrational motion of the molecules, the vibrationally resolved state-to-state and state-selective cross sections were obtained. The cross section variation with vibrational states is analyzed and the results of three collision orientations with $\Theta=0^\circ, 90^\circ$ and 180° manifestly elucidate the steric effect for H^+-CO and $\text{H}-\text{CO}^+$ collisions. The orientation-angle-averaged cross sections are in good agreement with experiments and it is shown that the electronic approximation may not be reliable for energies less than 100 eV/u. The large discrepancy between EA and IOSA calculations in the low-energy regime also reflects the significant influence of molecular vibrational motion. More experimental data for electron capture of protons with CO at energies less than 30 eV/u and for H collisions with CO^+ are needed.

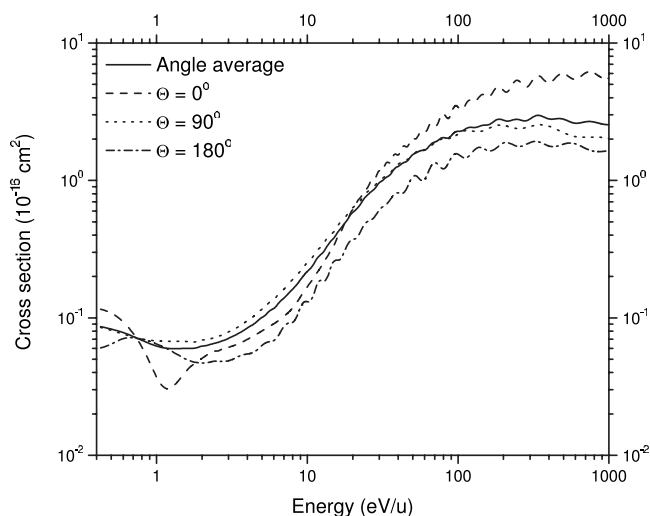


FIG. 14. Orientation-angle-averaged and orientation-angle-dependent total cross sections for the collisions of H with CO^+ .

ACKNOWLEDGMENTS

C.Y.L. and P.C.S. acknowledge support from NASA Grant No. NNG05GD98G and NSF Grant No. INT-0300708; R.J.B., J.P.G., Y.L., H.L., and P.F. acknowledge financial support from the Deutsche Forschungsgemeinschaft Grant

Bu 450/7-3; and M.K. acknowledges support from the Ministry of Education, Science, Sport, Culture and Technology, Japan Society for Promotion of Science (JSPS) for the US-JP Collaborative Research Program, and Collaborative Research Grant by National Institute for Fusion Science.

-
- [1] H. B. Gilbody and J. B. Hasted, *Proc. R. Soc. London, Ser. A* **238**, 334 (1956).
- [2] E. Gustafsson and E. Lindholm, *Ark. Fys.* **18**, 219 (1960).
- [3] W. Federer, H. Villinger, F. Howorka, W. Lindinger, P. Tosi, D. Bassi, and E. Ferguson, *Phys. Rev. Lett.* **52**, 2084 (1984).
- [4] R. S. Gao, L. K. Johnson, C. L. Hakes, K. A. Smith, and R. F. Stebbings, *Phys. Rev. A* **41**, 5929 (1990).
- [5] T. Kusakabe, K. Asahina, J. P. Gu, G. Hirsch, R. J. Buenker, M. Kimura, H. Tawara, and Y. Nakai, *Phys. Rev. A* **62**, 062714 (2000).
- [6] I. Čadež, J. B. Greenwood, A. Chutjian, R. J. Mawhorter, S. J. Smith, and M. Niimura, *J. Phys. B* **35**, 2515 (2002).
- [7] M. Kimura, J.-P. Gu, G. Hirsch, R. J. Buenker, and P. C. Stancil, *Phys. Rev. A* **61**, 032708 (2000).
- [8] P. C. Stancil, *Phys. Scr.*, T **T110**, 340 (2004).
- [9] T. J. D. Kumar, A. Saieswari, and S. Kumar, *J. Chem. Phys.* **124**, 034314 (2006).
- [10] V. Sidis, in *Advances in Atomic, Molecular, and Optical Physics*, edited by D. Bates and B. Bederson (Academic, New York, 1990), Vol. 26, p. 161.
- [11] M. Baer, in *State-Selected and State-to-State Ion-Molecule Reaction Dynamics*, edited by M. Baer and C.-Y. Ng (Wiley, New York, 1992), Part 2, p. 187.
- [12] R. J. Buenker and S. D. Peyerimhoff, *Theor. Chim. Acta* **35**, 33 (1974).
- [13] R. J. Buenker and S. D. Peyerimhoff, *Theor. Chim. Acta* **39**, 217 (1975).
- [14] R. J. Buenker, in *Proceedings of the Workshop on Quantum Chemistry and Molecular Physics, Wollongong, Australia*, edited by P. G. Burton (University of Wollongong, Wollongong, 1980), p. 1.5.1.
- [15] R. J. Buenker, in *Current Aspects of Quantum Chemistry*, edited by R. Carbo (Elsevier, Amsterdam, 1982), Vol. 21, pp. 17 and 81.
- [16] R. J. Buenker and R. A. Philips, *THEOCHEM* **123**, 291 (1985).
- [17] S. Krebs and R. J. Buenker, *J. Chem. Phys.* **103**, 5613 (1995).
- [18] T. H. Dunning, Jr., *J. Chem. Phys.* **90**, 1007 (1989).
- [19] P. H. Krupenie and S. Weissman, *J. Chem. Phys.* **43**, 1529 (1965).
- [20] I. Borges, Jr., P. J. S. B. Caridade, and A. J. C. Varandas, *J. Mol. Spectrosc.* **209**, 24 (2001).
- [21] C. Y. Lin, P. C. Stancil, J.-P. Gu, R. J. Buenker, and M. Kimura, *Phys. Rev. A* **71**, 062708 (2005).
- [22] L. B. Zhao, P. C. Stancil, J.-P. Gu, H.-P. Liebermann, P. Funke, R. J. Buenker, and M. Kimura, *Phys. Rev. A* **71**, 062713 (2005).
- [23] P. C. Stancil, D. R. Schultz, M. Kimura, J.-P. Gu, G. Hirsch, and R. J. Buenker, *Astron. Astrophys., Suppl. Ser.* **140**, 225 (1999).
- [24] P. C. Stancil, J.-P. Gu, C. C. Havener, P. S. Krstić, D. R. Schultz, M. Kimura, B. Zygelman, G. Hirsch, R. J. Buenker, and M. E. Bannister, *J. Phys. B* **31**, 3647 (1998).
- [25] B. Zygelman, D. L. Cooper, M. J. Ford, A. Dalgarno, J. Gerratt, and M. Raimondi, *Phys. Rev. A* **46**, 3846 (1992).
- [26] B. Zygelman, P. C. Stancil, N. J. Clarke, and D. L. Cooper, *Phys. Rev. A* **56**, 457 (1997).
- [27] V. Sidis, in *Collision Theory for Atoms and Molecules*, edited by F. A. Gianturco (Plenum, New York, 1989).
- [28] J. G. Wang, P. C. Stancil, A. R. Turner, and D. L. Cooper, *Phys. Rev. A* **69**, 062702 (2004).
- [29] L. Magnani and M. F. A'Hearn, *Astrophys. J.* **302**, 447 (1986).
- [30] S. A. Fuselier, E. G. Shelley, B. E. Goldstein, R. Goldstein, M. Neugebauer, W.-H. Ip, H. Balsiger, and H. Reme, *Astrophys. J.* **379**, 734 (1991).